Atorvastatin-Infused Carboxymethyl Cellulose-Gelatin Hydrogel: A Synergistic Strategy for Enhanced Wound Healing and Skin Tissue Regeneration

Seyed Reza Mousavi[1], Mojtaba Rashidi[2], Azam Khedri[1], Maryam Kouchak[3], Majid Salehi[4♯], Sepehr Zamani[5], Ghorban Mohammadzadeh[2*]

[1]Department of Clinical Biochemistry, School of Medicine, Ahvaz Jundishapur University of Medical Sciences, Ahvaz, Iran; [2]Hyperlipidemia Research Center, Department of Clinical Biochemistry, School of Medicine, Ahvaz Jundishapur University of Medical Sciences, Ahvaz, Iran; [3]Department of Pharmaceutics, Faculty of Pharmacy, Nanotechnology Research Center, Ahvaz Jundishapur University of Medical Sciences, Ahvaz, Iran; [4]Regenerative Medicine Research Center, Shahroud University of Medical Sciences, Shahroud, Iran; [5]Department of Tissue Engineering, School of Medicine, Shahroud University of Medical Sciences, Shahroud, Iran

How to cite:
Mousavi SR, Rashidi M, Khedri A, Kouchak M, Salehi M, Zamani S, Mohammadzadeh G. Atorvastatin-Infused Carboxymethyl Cellulose-Gelatin Hydrogel: A Synergistic Strategy for Enhanced Wound Healing and Skin Tissue Regeneration. *Iran. Biomed. J.* 2025; 29(3): 114-125.

ABSTRACT

Background: Skin tissue engineering is an innovative alternative to traditional methods for addressing skin defects. This study aimed to synthesize a hydrogel consisting of CMC and Gel containing ATR, which has the potential to accelerate tissue regeneration and wound healing in an animal model.

Methods: Five unique formulations of hydrogel with different concentrations of ATR (0.1%, 0.5%, 1%, and 2% w/v) were synthesized using CMC-Gel. The structural characteristics of the hydrogels were assessed using SEM and FTIR spectroscopy. Additional evaluations included swelling behavior, degradability, ATR release, compatibility, hemolytic activity, and the toxic effects on the viability of NIH/3T3 fibroblast cells. Their therapeutic effectiveness of these hydrogels in enhancing wound healing was investigated in an animal model by making a full-thickness skin incision in Wistar rats.

Results: The synthesized CMC-Gel scaffolds had a porous structure with interconnected pores measuring 103 ± 8.74 μm, with the ability to enhance cell migration. The MTT analysis showed a dose-dependent relationship between ATR and cell proliferation, and its desirable concentration was 0.1% w/v. Furthermore, increased ATR concentrations were associated with decreased dressing capacity for hemostasis and coagulation. In vivo studies revealed that all the hydrogel-treated groups significantly outperformed the gas-treated control group in promoting wound closure rates. Remarkably, the CMC-Gel-ATR 0.1% group exhibited the highest rates of wound closure, re-epithelialization, and angiogenesis.

Conclusion: Our results demonstrated that CMC-Gel-ATR may be proposed as a desirable wound dressing for clinical application due to its unique physicochemical properties and comprehensive biocompatibility in in vitro and in vivo investigations. ***DOI: 10.61186/ibj.5031***

Keywords: Angiogenesis, Atorvastatin, Biopolymers

Corresponding Author: Ghorban Mohammadzadeh
Hyperlipidemia Research Center, Department of Clinical Biochemistry, School of Medicine, Ahvaz Jundishapur University of Medical Sciences, Ahvaz, Iran; Tel.: (+98-911) 13436812; E-mail: mohammadzadeh@ajums.ac.ir; ORCID ID: 0000-0001-7921-4770

♯Co-corresponding author

List of Abbreviations:
ATR: atorvastatin; **BCI:** blood clotting index; **CMC:** carboxymethyl cellulose; **FBS:** fetal bovine serum; **FTIR:** fourier-transform infrared spectroscopy; **Gel:** gelatin; **H & E:** hematoxylin and eosin; **MTT:** 3'-(4,5-Dimethylthiazol-2-yl)-2,5-diphenyl tetrazolium bromide; **PBS:** phosphate-buffered saline; **SEM:** scanning electron microscopy

INTRODUCTION

Skin injuries are among the most common medical issues, often resulting in high medical costs, reduced individual productivity, and limited physical activities[1]. These injuries disrupt the normal function of the skin, causing the body to lose essential fluids and proteins, alter metabolic processes, and affect the circulatory and defense systems[2].

Traditionally, wound treatment strategies included natural substances such as honey and plant extracts. Today, numerous types of dressings have been developed to accelerate wound healing. One of the most significant advancements in dressing production is the use of polymeric materials. Among them, hydrogels have a special capability because of their three-dimensional network structure. Additionally, due to their fluid-absorption capacity, these materials can efficiently absorb exudate from wounds and making a moist wound environment[3].

CMC and Gel are two natural and semi-synthetic polymers that can be used to create biomedical hydrogels. CMC features attractive surface characteristics that enhance protein adsorption, facilitate cell aggregation and differentiation, and provide low degradation rates, high mechanical strength, and excellent biocompatibility. Furthermore, CMC can retain moisture in wound areas, which promote the growth of the extracellular matrix and the regeneration of the epithelium[4]. Gel, another biocompatible polymer produced by hydrolyzing collagen, provides several advantages, including biosafety, compatibility with biological systems, non-toxicity, and cost-effectiveness. Its amino acid sequences, such as RGD, enhance hemostasis and stimulate cell adhesion and proliferation throughout the healing process[5].

ATR is a member of the second generation of statins. In addition to the anti-inflammatory properties, statins are a viable option for wound healing as they can control cellular processes[6]. Studies have explored the effectiveness of statins in treating wounds and skin disorders using different formulations and administration methods, including intraperitoneal injection and oral intake. However, like other systemic medications, oral statins have side effects, including myopathy and liver problems[7]. Topical drug delivery approaches are suggested as a feasible substitute for oral statins in the wound healing process. This approach can minimize side effects, improve therapeutic effects, and enhance medication delivery[8].

The present study aimed to exhibit that the incorporation of ATR into a CMC-Gel hydrogel could enhance wound healing by modulating the wound microenvironment and improving tissue regeneration.

While the therapeutic potential of ATR has been well established, its integration into biopolymer-based topical scaffolds remains underexplored. We hypothesize that embedding ATR in a CMC-Gel scaffold can promote wound healing by enhancing moisture retention, supporting cell viability and proliferation, and facilitating tissue regeneration. This approach addresses the limitations of conventional treatments and contributes to the development of multifunctional, bioactive wound care systems. To our knowledge, the combination of CMC, Gel, and ATR in a topical hydrogel formulation has not been extensively investigated, representing a novel advancement in hydrogel-based wound healing approaches.

MATERIALS AND METHODS

Materials

CMC and Gel powder (bovine skin, type B) were purchased from Sigma-Aldrich (USA). Trypsin-EDTA, DMEM, FBS, and penicillin-streptomycin were supplied by Gibco (Germany). ATR was obtained from Raana Pharmaceutical Company (Tabriz, Iran). The Pasteur Institute of Iran in Tehran provided the fibroblast cell line NIH/3T3.

Synthesis of CMC-Gel and CMC-Gel-ATR Hydrogels

CMC powder (4% w/v) and Gel powder (3% w/v) were dissolved in deionized water (8:1 ratio) under stirring at 400 rpm for 12 hours at room temperature. ATR was then added and homogenized for six hours. Afterwards, phenoxyethanol was added to 0.9% of the final volume of the hydrogel to enhance stability and provide antiseptic properties (Table 1). The hydrogels were preserved at -80 °C for 16 hours and then transferred to a freeze dryer (Terrace, Spain) set at -54 °C for 48 hours, which allowed a porous structure to be formed[9].

Characterization of the scaffolds
Scanning electron microscopy

SEM was used to evaluate the surface properties of the generated lyophilized hydrogels (SEM; DSM 960A, Zeiss, Germany). To improve conductivity, a small layer of gold was applied to the freeze-dried hydrogels (SCD 004, Balzers, Germany). Image J and Origin Pro software were used to determine the average pore diameter. For this assessment, 20 of randomly chosen places within each image were scanned[10].

Table 1. Formulation of CMC-Gel-ATR for 1 mL of hydrogel

Hydrogel (sample)	Ratio CMC:Gel (% v/v)	Polymer Concentration (% w/v)	ATR Concentration (mg)	Phenoxyethanol (% v/v)
CMC-Gel	8:1	4:3	0	0.9
CMC-Gel-ATR 1 (0.1% w/v)	8:1	4:3	1	0.9
CMC-Gel-ATR 5 (0.5% w/v)	8:1	4:3	5	0.9
CMC-Gel-ATR 10 (1% w/v)	8:1	4:3	10	0.9
CMC-Gel-ATR 20 (2% w/v)	8:1	4:3	20	0.9

Fourier-transform infrared spectroscopy

FTIR was utilized to examine the interactions among functional groups in different hydrogel structures, particularly CMC-Gel and CMC-Gel-ATR. The FTIR spectroscopy technique (Spectrum GX, PerkinElmer, USA) was used to record the FTIR spectra spanning a wavelength range of 400 to 4000 cm^{-1}[11].

Evaluation of hydrogel degradation

The rate of degradation was assessed by measuring the weight loss of the hydrogel samples. Before submerging the dried hydrogels in a PBS solution (pH 7.4), we recorded their weights (W_0). The samples were then immersed in the PBS solution for predetermined intervals of 2, 6, 12, 24, and 48 hours. After each interval, excess solution was removed from the samples before reweighing them (W_1). The percentage of weight reduction was finally calculated using the formula given in Equation (1)[12].

$$\text{Weight loss (\%)} = \frac{W_0 - W_1}{W_0} \times 100 \qquad (1)$$

Evaluation of hydrogel water uptake

The ability of hydrogel samples to absorb water was evaluated at room-temperature. A freeze-drying procedure was used to lyophilize the hydrogels. The initial weights of the freeze-dried samples (W_0) were recorded before their immersion in PBS for varying periods (3, 6, 12, 24, and 48 hours). The samples were reweighed (W_1) at each specified time interval, and equation (2) was used to determine the water absorption[13].

$$\text{Water absorption (\%)} = \frac{W_1 - W_0}{W_0} \times 100 \qquad (2)$$

Evaluation of hydrogel blood compatibility

A 2 mL volume of rat blood was diluted with 2.5 mL of normal saline. The diluted blood sample (200 µl) was then added to three identical hydrogel samples (100 µL) prepared in 96-well plates. After 1 hour of incubation at 37 °C, the plates were centrifuged (1500 rpm, 10 minutes,). For the experimental controls, a negative control was prepared by combining 4 mL of normal saline with 200 µL of diluted blood, while a positive control was prepared by mixing 4 mL of distilled H$_2$O with 200 µL of diluted blood[14]. The supernatant was then tested for absorbance at 545 nm, and the percentage of hemolysis was determined using Equation (3).

$$\text{Hemolysis (\%)} = \frac{Ds - Dnc}{Dpc - Dnc} \times 100 \qquad (3)$$

Evaluation of hydrogel's BCI

Fresh rat blood was diluted in a citrated tube to measure the blood coagulation index of the samples. Next, 1.5 g of each sample was incubated at 37 °C for 1 hour. The samples were then combined with 100 µL of blood from rats. The mixture was incubated (5 minutes) before adding 0.2 M of CaCl$_2$. After an additional five minutes, each sample was mixed with 25 mL of distilled H$_2$O. The resultant suspensions were transferred to a 96-well plate for further analysis following a final incubation of five minutes. To create the control samples, we combined 25 mL of deionized H$_2$O with 100 µL of fresh human blood[15]. Using equation (4), we measured the relative absorbance of the hydrogel samples at 545 nm to calculate the BCI.

$$\text{BCI (\%)} = \frac{A\ sample}{A\ control} \times 100 \qquad (4)$$

Evaluation of hydrogel's cytotoxicity effects

The effect of CMC/Gel and CMC/Gel/ATR hydrogel dressing extracts on NIH/3T3 fibroblast cell line was carried out by using the MTT assay. The NIH/3T3 fibroblast cell line were seeded at a density of 1×10^4 cells per well in a sterile 96-well plate containing DMEM supplemented with 10% FBS. The cells were then incubated with 5% CO$_2$ at 37 °C overnight. To prepare hydrogel extracts, we incubated hydrogel samples containing different concentrations of ATR with DMEM for 48 hours under sterile conditions. After a 24-hour incubation period, 100 µL of the extracts were added to each well in triplicate. Following this incubation period, 20 µL of MTT solution (5 mg/mL^{-1})

116

was added to each well, and the supernatants were discarded. After three hours of further incubation at 37 °C, 100 μL of DMSO was added to dissolve the formazan crystals[16]. The absorbance at 570 nm was then measured using a plate reader to determine the percentage of cell viability, which was calculated using equation 5.

$$\text{Cell viability (\%)} = \frac{\text{absorbance of sample}}{\text{absorbance of control}} \times 100 \qquad (5)$$

Evaluation of release of ATR

To determine the amount of ATR released from the CMC-Gel hydrogel, a standard curve must be created for ATR using a range of 0.1 to 100 mg./mL^{-1}. CMC-Gel-ATR 1 mg/mL^{-1} hydrogel was placed in 5 mL of simulated body fluid within a shaker incubator kept at 37 °C (50 rpm). The absorbance of the supernatants was measured at 246 nm at different time intervals: 2, 4, 6, 12, 24, 36, 48, 72, and 96 hours, to evaluate the release of ATR[17]. Finally, by analyzing the established standard curve for ATR, we transformed the spectroscopic results into quantitative values.

Evaluation of hydrogel's pH variation

At predetermined intervals of 2, 4, 6, 12, 24, and hours, the pH of the normal saline containing the hydrogel samples was measured at room temperature using a digital pH meter (pH/mV Meter 502 7) to monitor any potential pH variations induced by the hydrogel[18].

In vivo experiment groups

Adults male Wistar rats (n = , weighing 200–250 g) were purchased from Shahroud University of Medical Sciences (Shahroud, Iran). The animals were provided food and water in standard housing conditions. The produced hydrogels were evaluated for their effectiveness in wound healing using a full-thickness wound model (1.5 × 1.5 cm^2). Rats were given an intraperitoneal injection of 100 mg/kg^{-1} of ketamine and 10 mg/kg^{-1} of xylazine to induce anesthesia. The dorsal skin of rats was cleaned, shaved, and disinfected using 70% alcohol. Afterwards, the rats were randomly divided into three groups of six. Group 1: negative control (treated with sterile gauze); Group 2: treated with CMC-Gel hydrogel; Group 3: treated with CMC-Gel-ATR hydrogel. The animals were sacrificed 14 days after the procedure, and the wound tissue was collected for histological analysis. Photographs taken 14 days following surgery were used to monitor the wound healing process[19]. Image J software was used to evaluate the results. Equation 6 was employed to calculate the percentages of wound closure.

$$\text{Wound closure (\%)} = 1 - \frac{\text{wound area}}{\text{initial area}} \times 100 \qquad (6)$$

Histopathological analysis

The development of granulation tissue, angiogenesis, scar formation, collagen deposition and re-epithelialization were assessed using Masson's trichrome and H&E staining. Tissue specimens were preserved in 10% formalin for histological examination. After being dehydrated and fixed in paraffin, the specimens were cut into 5 μm-thick sections[20]. We used a light microscope (Olympus BX51; Olympus, Tokyo, Japan) to analyze the histology slides.

Statistical analysis

GraphPad Prism 10 software was used for all statistical analyses. For normally distributed data, a one-way analysis of variance (ANOVA), followed by Tukey's post hoc was used for multiple group comparison. For non-normally distributed data, we applied the Kruskal–Wallis test, followed by the Mann–Whitney U test. Data are presented as mean ± SD. A *p* 05 was considered statistically significant.

RESULTS

Morphological properties of hydrogels

The SEM analysis of the CMC-Gel scaffold (Fig. 1A-1C) revealed a porous architecture characterized by larger pores (103 ± 8.74 μm), which may not be ideal for promoting cell adhesion and migration. In contrast, the CMC-Gel-ATR20 scaffold (Fig. 1D-1F) exhibited a finer porosity and a more consistent fibrous network (62.39 ± 5.07), offering an increased surface area for cell attachment. Recent research indicates that this characteristic is crucial for enhancing the regeneration of damaged tissues. Therefore, incorporating ATR into the CMC-Gel-ATR scaffold has improved its functional attributes.

FTIR spectral characteristics

Figure 1G and 1H show the results of FTIR spectra of CMC-Gel and CMC-Gel-ATR20 scaffolds. A broad band at 3400–3300 cm^{-1} corresponds to O–H and N–H stretching in CMC and Gel, respectively. The peak near 2900 cm^{-1} is from CMC and amide I from Gel, while 1550 cm^{-1} corresponds to the amide II band. The peak at 1420 cm^{-1} reflects symmetric COO$^-$ stretching, and the range between 1050 and 1100 cm^{-1} relates to C–O–C and C–O stretching. Shifts in these bands suggest hydrogen bonding between CMC and Gel, confirming their compatibility (Fig. 1G). For CMC-Gel-ATR20 (Fig. 1H), the peaks at 1695.04 and 1714.72 cm^{-1} indicate C=O stretching associated with ATR.
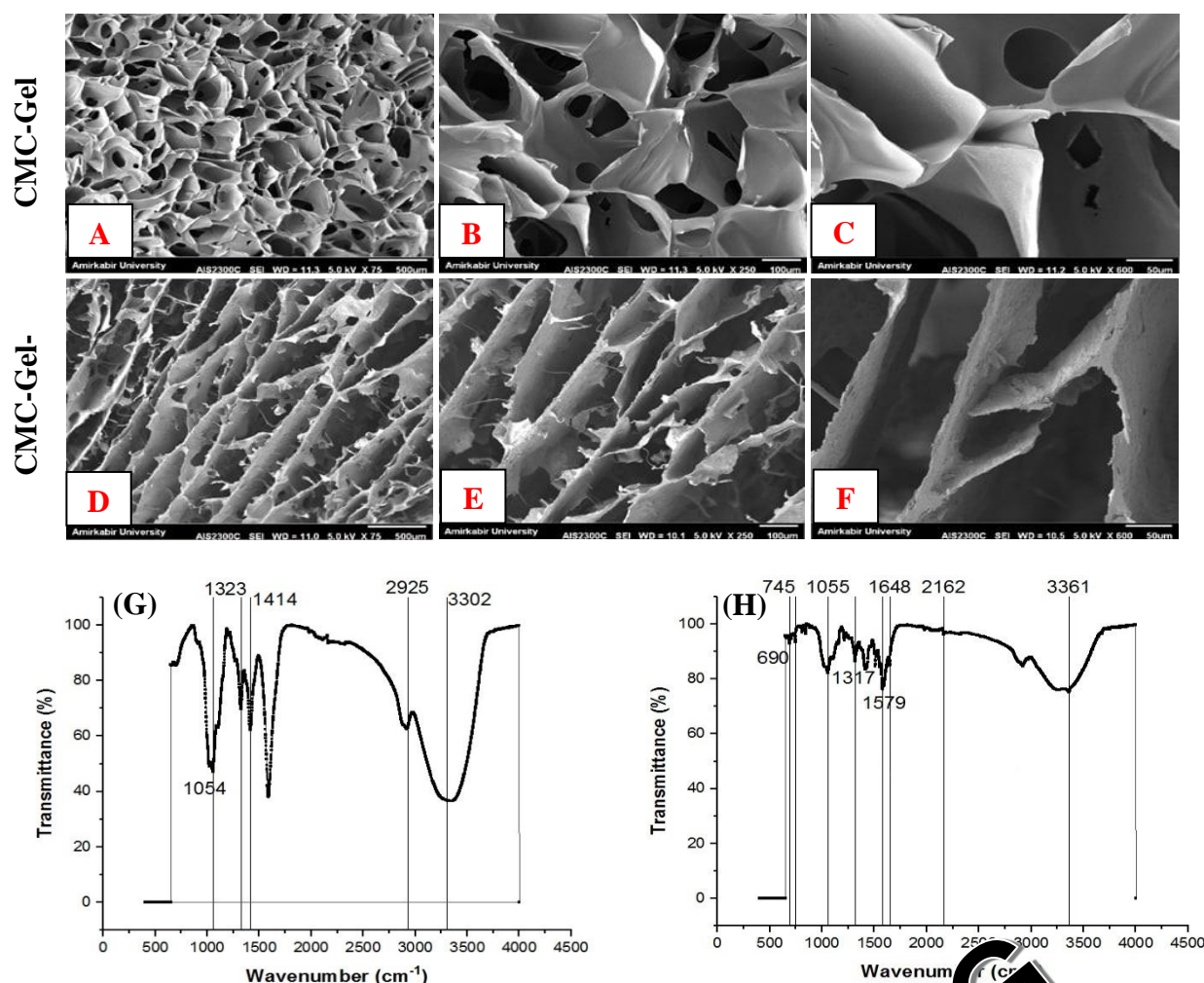
Fig 1. SEM of CMC-Gel (A, B, C) and , CMC-Gel-ATR (D, E, F) with 75×, 250×, and 500× magnif~~ic~~ation. FTIR spectrums of CMC-Gel (G) and CMC-Gel-ATR20 (H) at 400 to 4000 cm⁻¹.

Additional peaks at 1648.21 and 2162.04 cm⁻¹ likely correspond to conjugated C=C vibrations in aromatic rings. Bands at 1579.07, 1591.27, and 1517.63 cm⁻¹ further support the presence of aromatic structures. The 1404 to 1424 cm⁻¹ region relates to C–H bending or ester C–O stretching, and the 689.96 cm⁻¹ band confirms the presence of mono-substituted benzene rings. These findings affirm the successful incorporation of ATR.

Degradation behavior of hydrogels

The weight loss of the scaffolds was assessed at intervals of 2, 6, 12, 24, and 48 hours. CMC-Gel showed the highest degradation (98.0 ± 3.2 %) at 48 h, followed by CMC-Gel-ATR1 (94.5 ± 5.36%), ATR5 (93.5 ± 2.12%), ATR20 (88.5 ± 2.13%), and ATR10 (87 ± 4.24%). After 2 hours, the degradation rates were as follows: 22 ± 2.82% (CMC-Gel), 19 ± 1.41% (CMC-Gel-ATR1), 13.5 ± 2.12% (ATR5), 19.5 ± 0.78%

(ATR20), and 12.5 ± 0.79% (ATR10). Although the water absorption of ATR may influence scaffold degradation at higher doses, no statistically significant differences were observed among the treatment groups at any time point ($p > 0.05$). All comparisons were made relative to the CMC-Gel group.

Swelling behavior of hydrogels

All groups demonstrated a time-dependent increase in water uptake from 3 to 48 hours. CMC-Gel exhibited the highest swelling rates, reaching 16.5 ± 2.12%, 85.22 ± 10.21%, and 109.01 ± 12.94% at 3, 24, and 48 hours, respectively. Although ATR-containing hydrogels showed a similar swelling trend over time, a dose-dependent reduction in water absorption was observed. Following 48 hours, CMC-Gel-ATR1, ATR5, ATR10, and ATR20 reached 108 ± 10.53%, 96.5 ± 7.26%, 94 ± 6.05%, and 77.5 ± 3.92%,

118   *Iran. Biomed. J. 29 (3): 114-125*

respectively. Notably, the ATR20 showed a significant reduction in water uptake compared to CMC-Gel at both 24 hours and 48 hours ($67 \pm 2.82\%$ vs. $85.22 \pm 10.21\%$) ($p < 0.05$), while other groups did not exhibit any significant difference.

Hemolysis behavior of hydrogels

The hemolysis rate in the CMC-Gel was $4.71 \pm 1.39\%$. The ATR-containing groups showed a dose-dependent hemolysis rates as follows: ATR1 ($2.5 \pm 1.3\%$), ATR5 ($3.57 \pm 1.35\%$), ATR10 ($3.81 \pm 1.25\%$), and ATR20 ($5.47 \pm 1.49\%$). All treatment groups differed significantly from the negative control group, with a hemolysis rate of $0.2 \pm 0.1\%$ ($p < 0.05$). In contrast, the positive control showed a highly significant increase in hemolysis rate, $99.33 \pm 5.37\%$ ($p < 0.0001$). An increase in the ATR dosage resulted in the heightened hemolysis, implying that only ATR20 exhibited potential hemolytic effects.

BCI of hydrogels

The BCI value of the CMC-Gel scaffold was found to be $27.31 \pm 4.15\%$. A dose-dependent increase was observed in BCI at high concentrations of ATR. The BCI values for CMC-Gel-ATR1, ATR5, and ATR10 were $29.06 \pm 3.3\%$, $33.57 \pm 3.84\%$, and $37.84 \pm 4.25\%$, respectively, with no statistically significant differences compared to CMC-Gel ($p > 0.05$). However, the CMC-Gel-ATR20 demonstrated a significant increase in BCI ($44.39 \pm 6.70\%$; $p < 0.01$), indicating reduced clotting potential at higher ATR concentrations. The positive control showed a BCI value of $90.23 \pm 5.39\%$, which was highly significant different from the CMC-Gel ($p < 0.0001$). This outcome suggests the effectiveness of ATR as a wound dressing, which is highly dependent on

dosage, i.e. at high concentrations, it may not be effective for managing bleeding wounds.

Analysis of MTT assay results

The cytotoxic effects of the prepared hydrogels on the cell viability are presented in Figure 2. These results indicate that low levels of ATR can maintain and even improve the fibroblast viability, while higher ATR concentrations may impart cytotoxicity. Therefore, 0.1% ATR was chosen for the animal study.

ATR release analysis

The cumulative release profile of ATR over various time intervals is illustrated in Figure 3. The amount of the released ATR was quantified by constructing a standard release curve. After 12 and 24 hours, the recorded releases of ATR from the hydrogel were 614.91 ± 22.70 µg and 780.2 ± 25.41 µg, respectively, leading to a total release of 919.61 ± 14.33 µg over a four-day duration. These results suggest a gradual release of ATR from the CMC-Gel hydrogel, reaching a plateau phase after 96 hours (949.61 ± 33.24 µg). No additional release was observed at the 72 and 96-hour marks.

Analysis of hydrogel pH variation

Table 2 reports the pH values of the synthesized hydrogels over 48 hours. All groups, except for CMC-Gel (7.13 ± 0.40), were in the slightly acidic pH range ($6.22–6.81$).

In vivo wound healing findings

The study evaluated the efficacy of CMC-Gel and CMC-Gel-ATR1 hydrogels using a full-thickness wound model (Fig. 4A). The negative control, which its
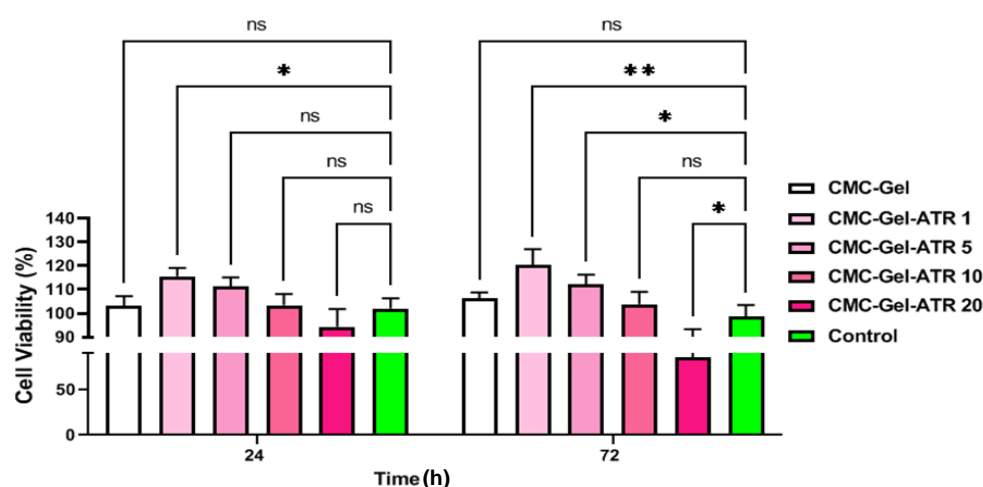

Fig 2. The cytotoxic effects of the prepared hydrogel on the 3T3 fibroblast viability measured by MTT assay at 24 and 72 h. Values represent the mean ± SD; n = 6; ns: not significant; $^*p < 0.05$, and $^{**}p < 0.01$.
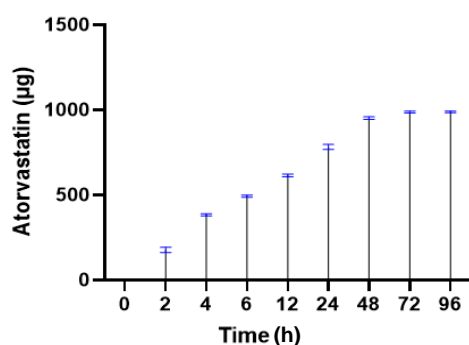
Fig 3. The release of ATR from CMC-gel hydrogel in PBS solution measured after 96 hours in a shaker incubator at 50 rpm at 37 °Cr. Values represent the mean ± SD (n = 3).

wounds had been covered with sterile gauze, exhibited signs of infection and inflammation, leading to incomplete healing after two weeks. In contrast, treated groups demonstrated significant healing during the same timeframe. Macroscopic photographic evaluations indicated that one-week post-treatment, the hydrogel groups experienced minimal bleeding. Notably, the CMC-Gel-ATR1 yielded the most promising outcomes, showing no indications of infection or inflammation. Figure 4B presents a quantitative analysis of wound healing based on the wound closure rates. The closure rates for the negative control, CMC-Gel, and CMC-Gel-ATR1 groups on days 7 and 14 were recorded as follows: 28.34 ± 10.66%, 70.21 ± 14.28%, 39.42 ± 14.39%, 87.66 ± 5.48%, 52.76 ± 9.71%, and 93.05 ± 6.17%, respectively. The CMC-Gel-ATR1 showed a significant improvement in wound healing compared to both the control and CMC-Gel groups. Both CMC-Gel and CMC-Gel-ATR1 groups displayed significant improvements compared to the control group on days 7 and 14; however, the effect was more pronounced in the CMC-Gel-ATR1 group ($p < 0.01$ vs. $p < 0.05$). This observation highlights the considerable potential of the CMC-Gel-ATR1 hydrogel in reducing healing time.

Histopathological findings

All treatment groups (negative control, CMC-Gel, and CMC-Gel-ATR1) demonstrated the formation of an distinct epidermal layer after 14 days. The CMC-Gel-ATR1 group showed thicker re-epithelialization and

more separation of the dermal layer (Fig. 5L). The CMC-Gel formed a crusty scab, which is a negative aspect of the healing process, as it was absent in the CMC-Gel-ATR1 group Fig. 5H). Blood vessel formation was more pronounced in both the negative control and CMC-Gel-ATR1 groups compared to the CMC-Gel group. However, many blood vessels in the negative control remained immature (Fig. 5C and 5L). Notably, only CMC-Gel-ATR1 group exhibited the development of skin appendages and resulted in a greater thickness of the dermis layer of the skin (Fig. 5J). The CMC-Gel-ATR1 was particularly successful in forming hair follicles (Fig. 5K). Additionally, an increased number of sebaceous glands was observed (Fig. 5K). Furthermore, collagen fiber synthesis was highest in CMC-Gel-ATR1 group (Fig. 5K). The findings from the Masson's trichrome study of all groups are shown in Figure 6. The formation of collagen fibers in the CMC-Gel-ATR1 group (Fig. 6K) was organized differently compared to the other groups.

DISCUSSION

Wound healing is a dynamic, multi-phase process. It begins with hemostasis, followed by the inflammatory and the proliferative phases, which aims to close the wound. During the remodeling phase, collagen fibers regenerate. Scaffolds made from CMC and Gel are favored for their biocompatibility, mechanical flexibility, and ability to replicate the extracellular matrix[21]. In a previous study, Soleimani et al. have investigated a hydrogel composed of CMC gel, revealing that it has adequate mechanical strength and antibacterial properties. Their study also verified that the hydrogel is non-toxic and plays a significant role in wound healing[22]. Saghafi et al. have demonstrated that topical application of the gel and nanogels containing ATR significantly accelerates wound healing and reduces pain without notable side effects, indicating ATR potential for wound management[8].

Studies of the effects of ATR on the survival and function of dermal fibroblasts are very limited. In one study, the treated human dermal fibroblasts with 0.5-2.5 μM of ATR showed no toxic effects after 24 h[23].

Table 2. pH values of the treated groups

Samples	0 h	2 h	4 h	6 h	12 h	24 h	48 h
CMC-Gel	7.18 ± 0.45	7.15 ± 0.39	7.14 ± 0.41	7.15 ± 0.43	7.14 ± 0.38	7.15 ± 0.41	7.13 ± 0.40
CMC-Gel-ATR 1	6.93 ± 0.24	6.84 ± 0.30	6.83 ± 0.28	6.83 ± 0.29	6.82 ± 0.31	6.82 ± 0.29	6.81 ± 0.24
CMC-Gel-ATR 5	6.85 ± 0.25	6.82 ± 0.29	6.82 ± 0.22	6.81 ± 0.26	6.85 ± 0.25	6.82 ± 0.29	6.82 ± 0.22
CMC-Gel-ATR 10	6.72 ± 0.19	6.70 ± 0.22	6.69 ± 0.20	6.68 ± 0.19	6.85 ±0.25	6.82 ± 0.29	6.82 ± 0.22
CMC-Gel-ATR 20	6.35 ± 0.36	6.28 ± 0.25	6.26 ± 0.19	6.25 ± 0.23	6.69 ±0.15	6.67 ± 0.17	6.66 ± 0.16

Values represent the mean ± SD (n = 6).
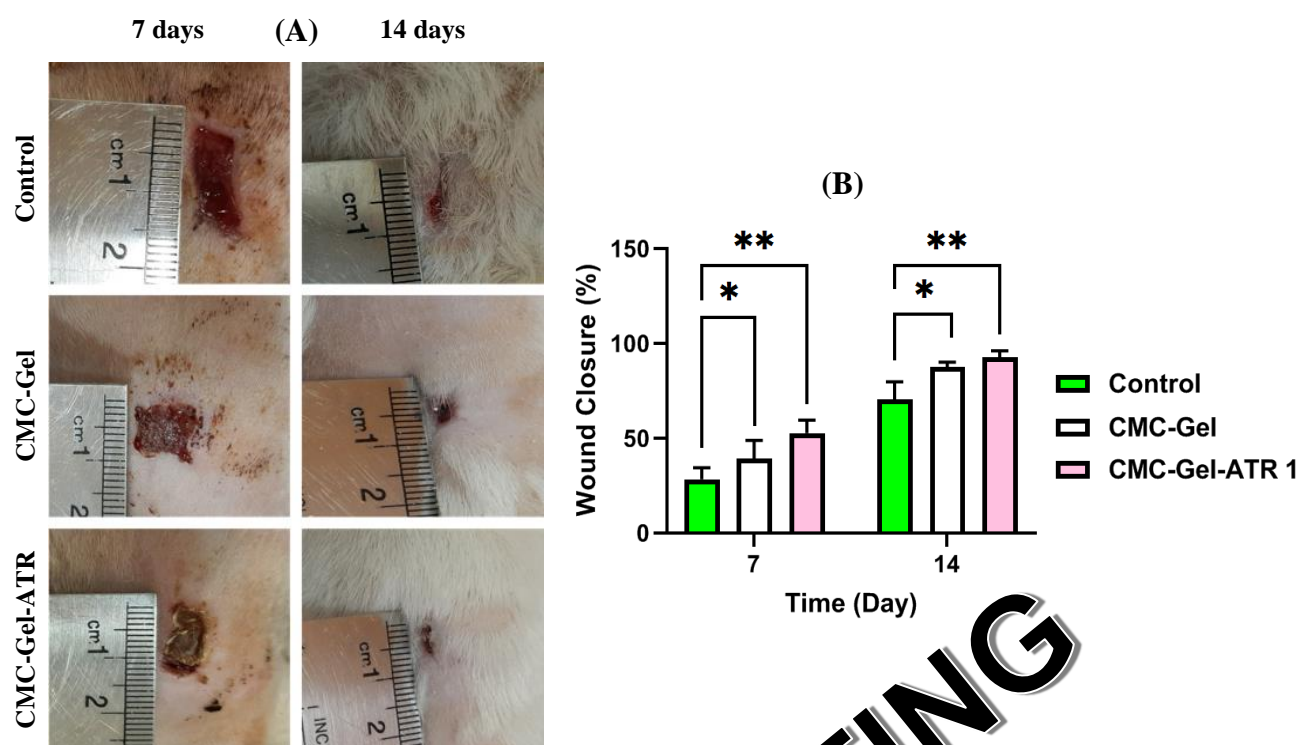
7 days   **(A)**   14 days

Fig 4. (A) In vivo wound-healing results; a macroscopic appearance of wounds treated with sterile gauze, CMC-Gel, and CMC-Gel-ATR1 hydrogels at 7 and 14 post-wounding; (B) a histogram comparing the percentage of wound closure among the experimental groups after 7 and 14 days following the initial wound. Values represent the mean ± SD (n = 6); $^*p < 0.05$, $^{**}p < 0.01$.

Another study has reported that concentrations more than 20 μM for 72 h, could significantly decrease viability due to oxidative stress and suppression of antioxidant enzymes[24]. MTT results from our study support that lower ATR concentrations are safer, while higher doses show cytotoxicity. Reports have suggested that pore sizes between 50 to 10 μm are optimal for wound healing because they facilitate effective cell migration. Our scaffolds exhibited pore sizes within this optimal range, suggesting their potential to support efficient cell migration and nutrient exchange[24]. Gradual degradation of the scaffolds is crucial to avoid inflammation from residual materials and support cell growth. 26. The scaffolds retained favorable biodegradability characteristics even after drug incorporation. CMC and gel scaffolds absorb and retain moisture due to their hydrophilic and porous structure, aiding chronic wound management. Moisture retention not only prevents wound dryness but also enhances the controlled release of ATR. Likewise, scaffold swelling influences drug permeability and diffusion rate [25].

Water uptake analysis confirmed the ability of hydrogels to maintain a moist environment, which is essential for healing[22]. The initial interaction between the implanted wound dressing and red blood cells induces an inflammatory response. Zhou and Yi have corroborated that the acceptable hemolysis threshold for wound dressings is below 5%[14]. Blood compatibility results of our study showed that all formulations remained below the critical 5% hemolysis threshold, except for ATR20. This finding indicates a dose-dependent hemocompatibility, which is essential for clinical applications. Platelet aggregation and coagulation are crucial for hemostasis, with a higher BCI suggesting slower clotting and enhanced blood compatibility[25]. A trial involving hypercholesterolemia patients has found that 24 weeks of ATR administration reduces mean platelet volume and the neutrophil-to-lymphocyte ratio, suggesting antiplatelet and anti-inflammatory effects of ATR[26]. Thus, the use of ATR in wound dressings is dose-dependent in which high doses can impair clotting and are unsuitable for treating bleeding wounds.

The range of pH of the wound environment plays a critical role in the healing process. The alkaline pH range (7.15–8.9), which are common in chronic wounds, slow down healing. However, an acidic environment promotes healing. Based on our results, all ATR-loaded samples showed acidic pH, which supports wound healing[27]. In vivo data corroborated our in vitro findings, showing that ATR at a concentration of 1 μM
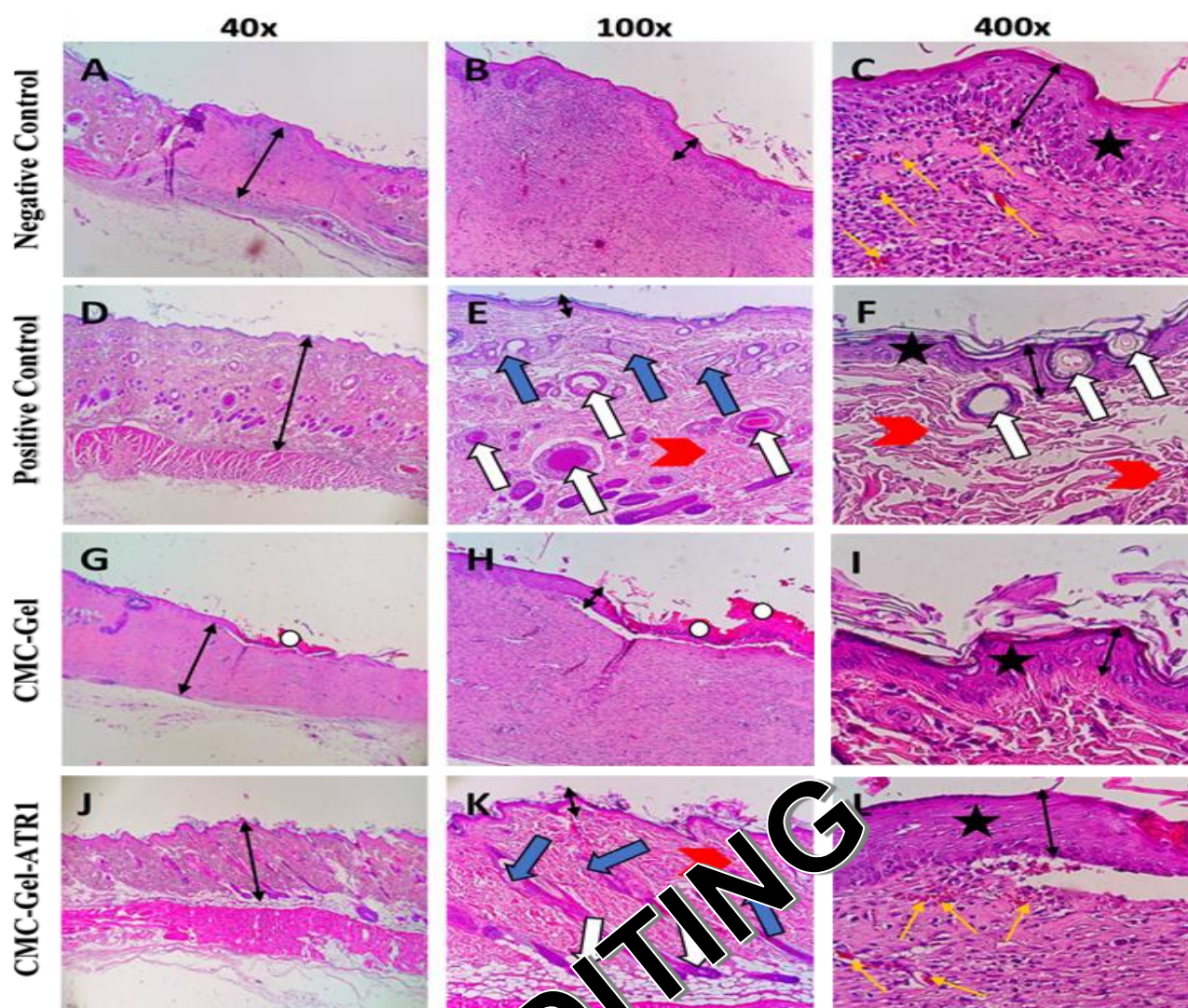
Fig 5. Microscopic sections of the healed incision wounds stained with H & E on day 14. Negative control (A, B, C); positive control (D, E, F); CMC-Gel hydrogel (G, H, I); CMC-Gel-ATR1 hydrogel (J, K, L). Black stars: epithelialization, white arrows: hair follicle, blue arrows: sebaceous glands, red arrowheads: mature collagen, yellow arrows: neovasculation.

accelerates wound closure and reduces inflammation. Histological outcomes confirmed that the CMC-Gel-ATR1 is more similar to the positive control in terms of organized epithelialization, vascularization, appendage formation, and collagen maturity.

ATR shows considerable promise for wound healing; however, caution is warranted regarding the disadvantages and limitations noted in the research, particularly the formulation of appropriate drug dosages. This study was limited to full-thickness cutaneous wounds and did not address chronic or complex wound types, such as burns, pressure ulcers, or diabetic wounds, which represent clinical challenges.

CONCLUSION

In this study, CMC-Gel and CMC-Gel-ATR hydrogels were successfully synthesized and evaluated as promising wound dressing compounds. Their physicochemical characteristics, cell viability, and in vivo wound healing properties were examined and supported by histological analysis. Morphological results confirmed the existence of a porous structure consisting of interconnected pores as well as loaded ATR, which are favorable for cell attachment and migration. The CMC-Gel-ATR hydrogel showed desirable properties for wound healing, including moisture absorption, biodegradability, desirable pH, BCI, and blood compatibility. Moreover, both ATR-free
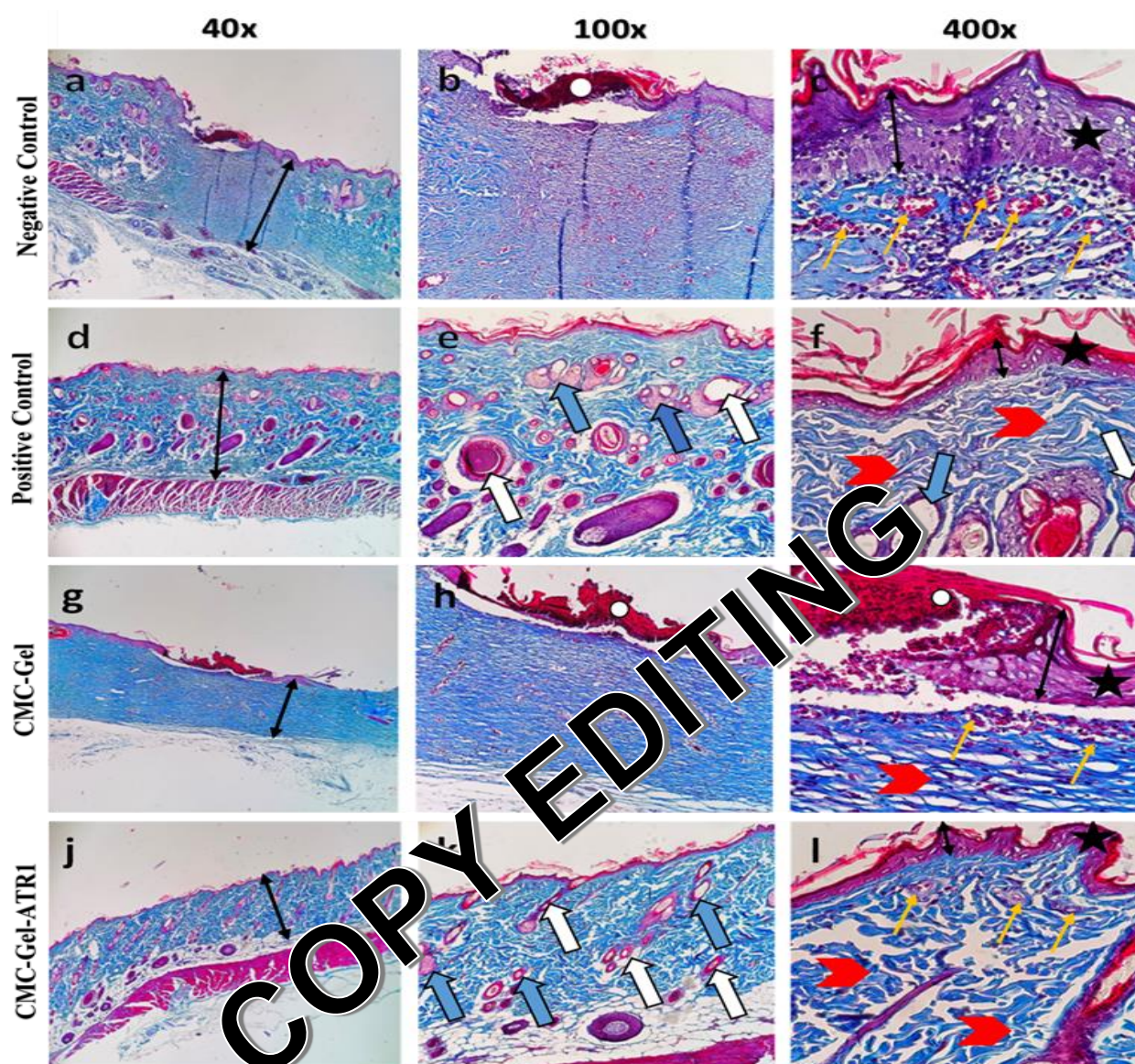
Fig 6. Microscopic sections of with the healed incision wounds stained with Masson's trichrome on day 14. Negative control (A, B, C), positive control (D, E, F); CMC-Gel hydrogel (G, H, I); CMC-Gel-ATR1 hydrogel (J, K, L). Black stars: epithelialization, white arrows: hair follicle, blue arrows: sebaceous glands, red arrowheads: mature collagen, yellow arrows: neovasculation.

and ATR-loaded hydrogels showed no cytotoxic effects on NIH/3T3 fibroblast cells. Animal studies in rat models showed that skin wounds treated with both hydrogels accelerated wound healing within 7 and 14 days. Histological results demonstrated that the hydrogel wound dressings significantly promoted organized epithelialization, vascularization, and collagen maturity, thus accelerating the general wound healing process. Overall, CMC-Gel-ATR wound dressing has many desirable properties for wound healing in clinical applications.

DECLARATIONS

Ethical approval

Animal experiments were approved by the Ethics Committee of Ahvaz Jundishapur University of Medical Sciences, Ahvaz, Iran (ethical code: IR.AJUMS.REC. 1402.513). All experimental procedures were carried out in accordance with the guidelines set forth by the Ethical Standards Committee of Shahroud Medical University, Shahroud, Iran (ethical code: IR.SHMU. REC.1398.157).

Consent to participate

Not applicable.

Consent for publication

All authors have approved the manuscript and agree with its submission to IBJ.

Authors' contributions

SRM: performed experiments, evaluated the data, discussed the results and strategy, and prepared the article draft; MR, AK and MK: contributed in a part of the project management; MS designed and managed the study; SZ: performed experiments, evaluated the data, discussed the results and strategy, and prepared the article draft; GM: designed and managed the study.

Data availability

All relevant data can be found within the manuscript.

Competing interests

The authors declare no conflict of interest.

Funding

This work was supported by Hyperlipidemia Research Center, Ahvaz Jundishapur University of Medical Sciences, Ahvaz, Iran [grant no. HLRC-0207].

Supplementary information

The online version does not contain supplementary material.

REFERENCES

1. Griffiths CE, Barker J, Bleiker TO, Hussain W, Simpson RC, editors. Rook's textbook of dermatology, 4 Volume Set, 10th Edition. Wiley-Blackwell; 2024.
2. Farahani M, Shafiee A. Wound healing: From passive to smart dressings. Adv Healthc Mater. 2021;10(16):2100477.
3. Levine JM, Delmore B, Cox J. Skin failure: Concept review and proposed model. Adv Skin Wound Care. 2022;35(3):139-48.
4. 4. Rahman MS, Hasan MS, Nitai AS, Nam S, Karmakar AK, Ahsan MS, et al. Recent developments of carboxymethyl cellulose. Polymers. 2021;13(8):1345.
5. Kang JI, Park KM. Advances in gelatin-based hydrogels for wound management. J Mater Chem B. 2021;9(6):1503-20.
6. Feingold KR. Cholesterol lowering drugs. In: Feingold KR, Ahmed SF, Anawalt B, Blackman MR, Boyce A, Chrousos G, Corpas E, de Herder WW, Dhatariya K, Dungan K, Hofland J, Kalra S, Kaltsas G, Kapoor N, Koch C, Kopp P, Korbonits M, Kovacs CS, Kuohung W, Laferrère B, Levy M, McGee EA, McLachlan R, Muzumdar R, Purnell J, Rey R, Sahay R, Shah AS, Singer F, Sperling MA, Stratakis CA, Trence DL, Wilson DP, editors. 2024. Endotext [Internet]. South Dartmouth (MA): MDText.com, Inc.; 2000–. PMID: 27809434
7. Zahedipour F, Hosseini SA, Reiner Z, Tedeschi-Reiner E, Jamialahmadi T, Sahebkar A. Therapeutic effects of statins: Promising drug for topical and transdermal administration. Curr Med Chem. 2024;31(21):3149-66.
8. Saghafi F, Ramezani V, Jafari Nedooshan J, Zarekamali J, Kargar S, Tabatabaei SM, et al. Efficacy of topical atorvastatin-loaded emulgel and nano-emulgel 1% on post-laparotomy pain and wound healing: A randomized double-blind placebo-controlled clinical trial. Int Wound J. 2023;20(10):4006-14.
9. Zamani S, Salehi M, Abbaszadeh-Goudarzi G, Chabok Gharagha D, Ehterami A, Esmaili S, et al. Evaluation effect of alginate hydrogel containing losartan on wound healing and gene expression. J Biomater Appl. 2025;39(7):762-88.
10. Hoque J, Prakash RG, Paramanandham K, Shome BR, Haldar J. Biocompatible injectable hydrogel with potent wound healing and antibacterial properties. Mol Pharm. 2017;14(4):1218-30.
11. Karvinen J, Kellomäki M. Characterization of self-healing hydrogels for biomedical applications. Eur Polym J. 2022;181:111641.
12. Xu Y, Chen H, Fang Y, Wu J. Hydrogel combined with phototherapy in wound healing. Adv Healthc Mater. 2022;11(16):2200494.
13. Sideek SA, El-Nassan HB, Fares AR, Elkasabgy NA, ElMeshad AN. Cross-linked alginate dialdehyde/chitosan hydrogel encompassing curcumin-loaded bilosomes for enhanced wound healing activity. Pharmaceutics. 2024;16(1):90.
14. Zhou C, Yi Z. Blood-compatibility of polyurethane/liquid crystal composite membranes. Biomaterials. 1999;20(22):2093-9.
15. Dawit H, Zhao Y, Wang J, Pei R. Advances in conductive hydrogels for neural recording and stimulation. Biomater Sci. 2024;12(11):2786-800.
16. Buranaamnuay K. The MTT assay application to measure the viability of spermatozoa: A variety of the assay protocols. Open Vet J. 2021;11(2):251-69.
17. Hamache T, Belboukhari N, Sekkoum K. Stereochemical of atorvastatin drug by using spectroscopic. Analysis. Clinical Trials and Case Studies. 2024;3(1):1-4.
18. Tavakoli J, Tang Y. Hydrogel based sensors for biomedical applications: An updated review. Polymers. 2017;9(8):364.
19. Salehi M, Ehterami A, Farzamfar S, Vaez A, Ebrahimi-Barough S. Accelerating healing of excisional wound

with alginate hydrogel containing naringenin in rat model. Drug Deliv Transl Res. 2021;11:142-53.

20. Arabpour Z, Abedi F, Salehi M, Baharnoori SM, Soleimani M, Djalilian AR. Hydrogel-based skin regeneration. Int J Mol Sci. 2024;25(4):1982.

21. Liang Y, He J, Guo B. Functional hydrogels as wound dressing to enhance wound healing. ACS Nano. 2021;15(8):12687-722.

22. Soleimani Z, Baharifar H, Najmoddin N, Khoshnevisan K. Evaluation of carboxymethyl cellulose/gelatin hydrogel-based dressing containing cefdinir for wound healing promotion in animal model. Gels. 2025;11(1):38.

23. Abootorabi S, Akbari J, Saeedi M, Seyedabadi M, Ranaee M, Asare-Addo K, et al. Atorvastatin entrapped noisome (Atrosome): Green preparation approach for wound healing. AAPS Pharm Sci Tech. 2022;23(3).

24. Marcheggiani F, Cirilli I, Orlando P, Silvestri S, Vogelsang A, Knott A, et al. Modulation of Coenzyme Q10 content and oxidative status in human dermal fibroblasts using HMG-CoA reductase inhibitor over a broad range of concentrations. From mitohormesis to mitochondrial dysfunction and accelerated aging. Aging. 2019;11(9):2565-82.

25. Montazerian H, Davoodi E, Baidya A, Baghdasarian S, Sarikhani E, Meyer CE, et al. Engineered hemostatic biomaterials for sealing wounds. Chem Rev. 2022;122(15):12864-903.

26. Akin F, Ayca B, Kose N, Sahin I, Akin MN, Canbek TD, et bal. Effect of atorvastatin on hematologic parameters in patients with hypercholesterolemia. Angiology. 2013;64(8):621-5.

27. Proksch E. pH in natur hue s and skin. J Dermatol. 2018;45(9):1044-5.